

Microstrip Line Test and Results

Simone Mencarelli

August 23, 2023

1 Relevant documents

[Doc1] S.M., “*Microstrip Line Characterization*”, August 2023

2 Introduction



Figure 1: Shortest (40 mm) line test fixture. Front: 5 mm x 40 mm adhesive copper trace on glass fiber panel. Back: thru-hole SMA connector with m2.5 screws and bolts.

This report contains the results for the microstrip line test produced using vector measurements of the reflection and transmission frequency response of three test fixtures of different lengths. The shorter fixture is shown in Fig. 1. The three fixtures feature a microstrip line built using an adhesive copper strip 5 mm wide on a piece of dielectric composite (Material Under Test) glued on a supporting aluminium slab. Two thru-hole connectors are bolted to the structure with the central pin trimmed to length and soldered to the copper line. From here on, the fixtures are referred to by their line length; respectively: long = 219 mm (L), medium = 146 mm (M), and short = 40mm (S).

The complex propagation coefficient γ extraction procedure is defined in

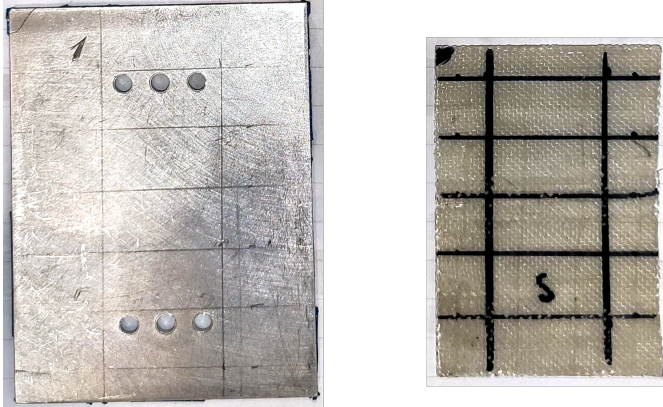


Figure 2: Measurement grids, two lines of points on the right and left side of the fixture at 1.5 cm from the edge.

[Doc1] and applied here with minor modifications. An overview of the methodology and the results of this de-embedding procedure are reported in Section 4.

The error sensitivity to small differences in the average permittivity of the fixtures is derived in Section 5 in an effort to explain the discrepancies found in the results of Section 4.

The procedure for fitting the measured datum to a CST microstrip model is reported in Section 6 along with the resulting permittivity and loss tangent of the *Material Under Test* (MUT).

The conclusions are drawn in Section 7.

3 Fixtures assembly and geometrical variability

The test fixtures were assembled by gluing the MUT onto the support aluminium slab (of 1.17mm in thickness) using some superglue. To evaluate the thickness of the dielectric material to be tested and the layer of glue, several measurements were taken using a micrometer (0.01 mm resolution)

| Fixture | Samples | Left MUT | | Right MUT | | Total left | | Total right | |
|---------|---------|----------|----------|-----------|----------|------------|----------|-------------|----------|
| | | E | σ | E | σ | E | σ | E | σ |
| L | 21 | 0.5140 | 0.0233 | 0.5195 | 0.0212 | 1.7802 | 0.0239 | 1.7667 | 0.0105 |
| M | 14 | 0.5118 | 0.0198 | 0.5309 | 0.0282 | 1.8492 | 0.0406 | 1.7935 | 0.0153 |
| S | 5 | 0.5088 | 0.0242 | 0.5163 | 0.0143 | 1.789 | 0.0201 | 1.748 | 0.0434 |

| Fixture | Samples | Dielectric (tot) left | | Dielectric (tot) right | | Glue left | | Glue right | |
|---------|---------|-----------------------|----------|------------------------|----------|-----------|----------|------------|----------|
| | | E | σ | E | σ | E | σ | E | σ |
| L | 21 | 0.6095 | 0.0252 | 0.5962 | 0.0109 | 0.0955 | 0.0303 | 0.0767 | 0.0221 |
| M | 14 | 0.6793 | 0.0406 | 0.6236 | 0.0153 | 0.1675 | 0.0396 | 0.0926 | 0.0330 |
| S | 5 | 0.62 | 0.02 | 0.566 | 0.058 | 0.1 | 0.0307 | 0.047 | 0.0699 |

Table 1: Assemblies thicknesses average and standard deviation, all values are in [mm].

on a regular grid of points distributed on two lines on the right and left side of the fixture as in Fig. 2.

The results of this measurement, an the inferred total dielectric thickness and glue thickness are tabulated in Table 1 in terms of average value E and standard deviation σ .

4 De-embedding results

The de-embedding results (virtual transmission line properties) are here presented in terms of:

- Transmissivity, i.e., the S21 of the de embedded length of transmission line, denoted with t .
- Reflectivity, i.e., the S21 of the de embedded length of transmission line, denoted with s .
- Effective permittivity ε_{eff} .
- Effective loss tangent $\tan \delta_{eff}$.

The effective permittivity and loss tangent are for visualization purposes only and are formulated from the low-loss approximation [1] for transmission lines (assuming all loss lumped into the dielectric material and the phase velocity independent of loss).

The effective permittivity is given by

$$\varepsilon_{eff} = \left(\frac{c[\text{unwrap}(\angle t) + n2\pi]}{2\pi f L} \right)^2, \quad (1)$$

where c is the speed of light, L is the line length (length difference between the two fixtures), f is the frequency and n an integer to correctly reconstruct the true-time phase delay (usually $n=0$ if the first sample of f is small enough).

The loss tangent is defined as

$$\tan \delta_{eff} = -\frac{\ln(|t|)c}{L\pi f \sqrt{\varepsilon_{eff}}}. \quad (2)$$

A better figure that can be used to make the measurement results independent from the physical length L , is the complex propagation constant

$$\gamma = \alpha + j\beta = \ln(t)/L, \quad (3)$$

used in Section 6 to match the CST model to the measured data.

Note how all the above depend (measurand) exclusively on the transmissivity t . While, the reflectivity s , using the de-embedding procedure of [Doc1], can be considered as a function of the de-embedding error, as it should be 0 in the ideal case.

For the measured data, it was noted that the response s varies changing the gate width from the, originally considered, distance between two reflections to a smaller value. Since this changes improves or degrades the value of s in different parts of the spectrum, it was chosen to modify the de-embedding algorithm of [Doc1], to sweep over several values for the gate width and then perform a weighted average of the different resulting t -curves using the s -curves as a logarithmic weighting factors for every frequency bin .

This sensibility to changes in the gates widths is probably due to some irregularities in the measured transmission lines, far from being perfectly homogeneous due to the manufacturing process. This change in gate length, in theory, should not impact negatively on the overall result as it is equivalent to performing a low-pass filtering of the time impulse response of the transitions to be removed. In fact, the average s value over frequency reduces when this weighted average technique is introduced.

Moreover, instead of always using the longer transmission line to generate the transition scattering matrices to de-embed the shorter transmission line, all combinations of measurement/simulation pairs are computed. Although using the longer line as reference provides the best theoretical frequency resolution, is interesting to see what happens in the reversed case where the transition scattering parameters have a naturally shorter (low-pass) time response, and hence a smoother shape in frequency.

The resulting de-embedded virtual lines can therefore either have a causal or an anti-causal response. For ease of comparison all the signs in the data plots are normalized to always represent the equivalent anti-causal transmission lines, e.g., “LS” is the *anti-causal* (negative length) line obtained de-embedding the line S from the transitions T-matrices obtained from the response of L, and vice versa “SL” is the *causal* line of identical positive length.

4.1 Simulated data baseline

In order to validate the modified de-embedding algorithm, a run wit simulated data, from the same CST models of [Doc1] was performed. To observe the effect of the weighted average step, one run for the de-embedding algorithm is set to use the widest possible gate (as in [Doc1]). The S-parameter results in Fig. 3 show that the averaging slightly improves on the ripple and the s response (especially at the edges) wile not changing substantially the response. The permittivity, Fig. 4, and loss tangent Fig. 5, results are compared with the equivalent values computed form the complex propagation constant of the waveguide port mode solver of CST, and from a full-wave

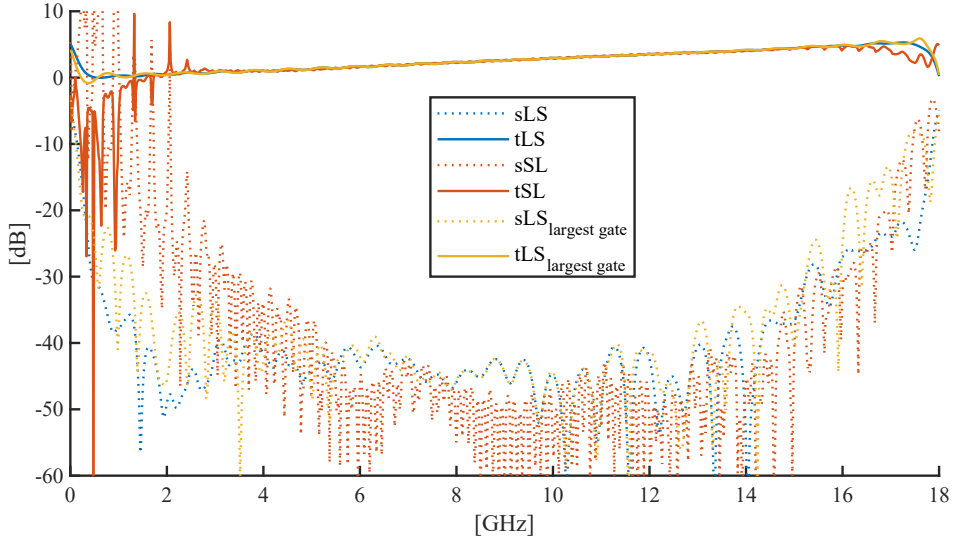


Figure 3: De-embedding results from full wave simulations of a 40 mm (S) and a 219 mm (L) test fixtures. Solid lines: transmissivity (s), dotted lines: reflectivity (t); for all the combinations plus LS deembeding without gate width variation. The transmissivity sign is chosen to always correspond to a negative-length section of lossy transmission line (for ease of comparison).

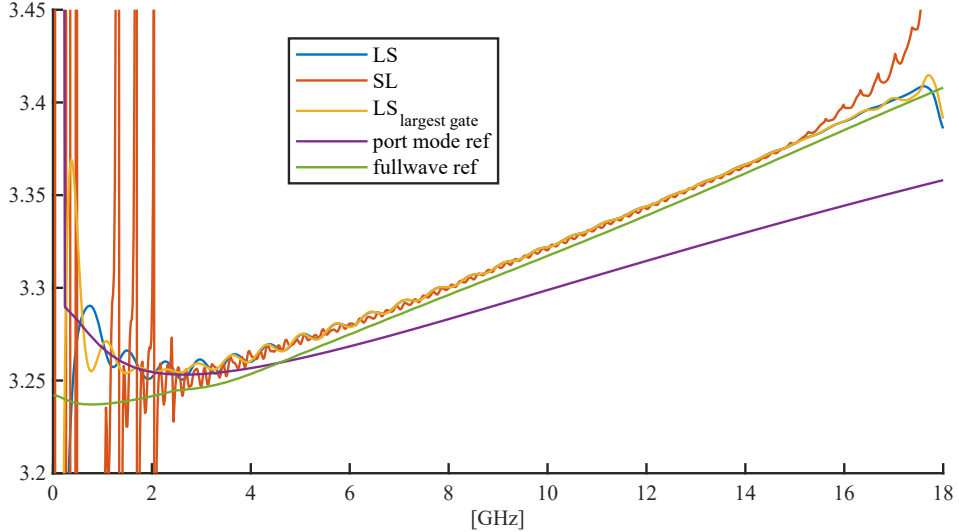


Figure 4: Simulated data retrieved effective permittivity compared with ε_{eff} calculated from the S_{21} of a full-wave simulation of a microstrip section (terminated on adaptive waveguide ports), and effective dielectric constant computed by the port mode solver of CST.

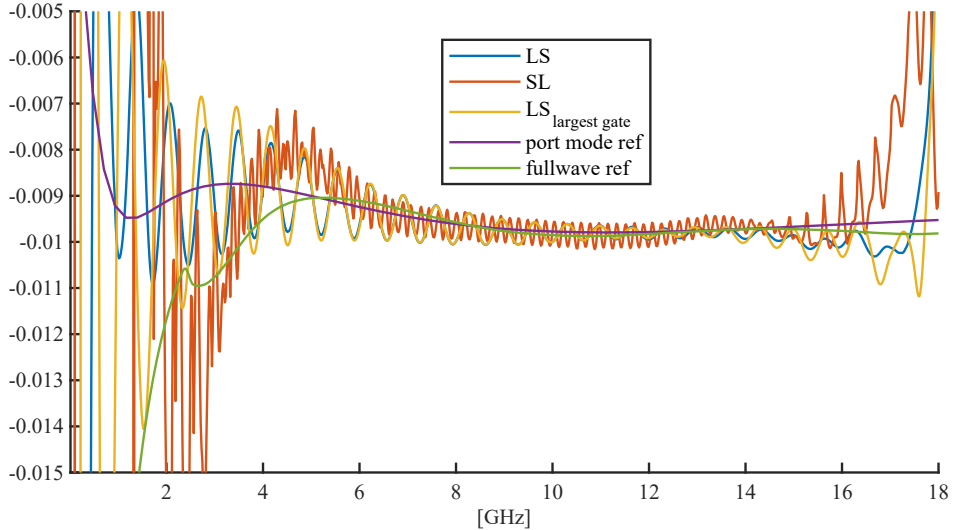


Figure 5: Simulated data retrieved effective loss tangent compared with $\tan \delta_{eff}$ calculated from the S_{21} of a full-wave simulation of a microstrip section (terminated on adaptive waveguide ports), and effective loss tangent computed by the port mode solver of CST.

simulation of a section of microstrip line terminated on to two adaptive waveguide ports.

The reason behind the large difference between the port mode solver result and the full wave solution in Fig. 4 is unclear. The slight difference between the de-embedding results and the full wave result (in Fig. 4), instead, might be caused by a phase error due to finite meshing of the model or other numerical inaccuracies. The full-wave reference should be in any case the most accurate representation of the de-embedded virtual line and the total error appears reasonably small.

The results in Fig. 5 seem all to be in good agreement (at least in the central portion of the spectrum), with ripple and *edge diffraction* effects that seem to be most severe in the “SL” case.

4.2 Measurements

The measurements are made connecting the test fixtures to the PNA with two APC7 to APC3.5 adapters. The instrument is calibrated at the APC7 interface, there is no need to calibrate the 3.5 connectors as they can be considered as part of the transition to be removed during the de-embedding by performing two measurements for every fixture as described here.

For every fixture, two measurements are taken. The first with the port 1 of the PNA connected to the port 1 of the fixture (e.g., marked in Fig. 1) and port 2 of the PNA to the port 2 of the fixture. In the second measurement,

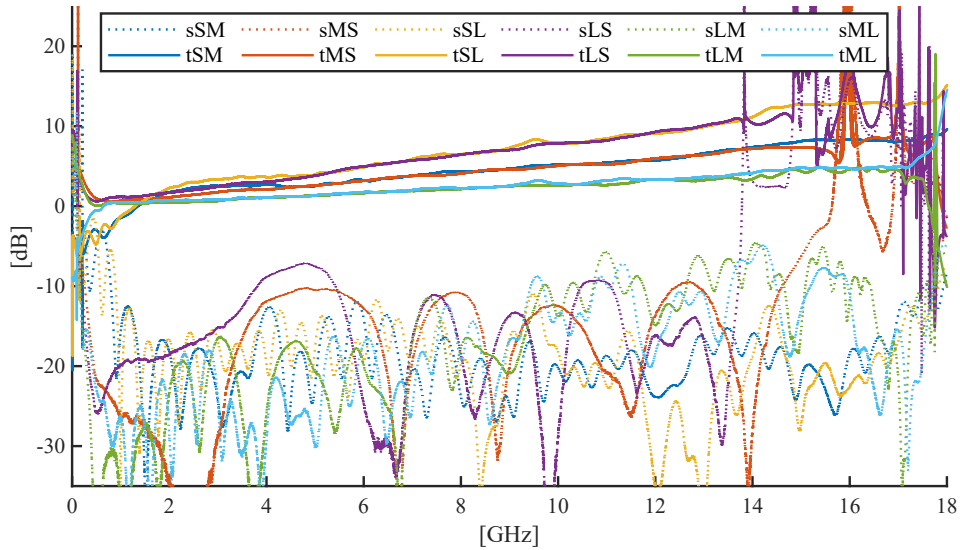


Figure 6: De-embedding results from the measurements of the test fixtures. Solid lines: transmissivity (s), dotted lines: reflectivity (t); for all the reference-fixture – under-test-fixture combinations e.g. LS = long line as reference and short line de-embedding target. The transmissivity sign is chosen to always correspond to a negative-length section of lossy transmission line (for ease of comparison).

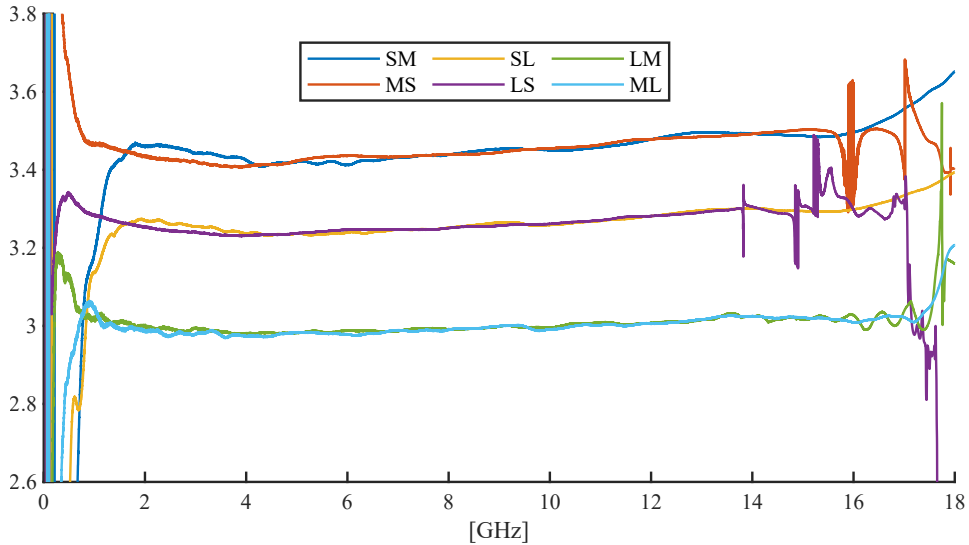


Figure 7: Measured data retrieved effective permittivity for all the reference-fixture – under-test-fixture combinations.

the fixture is rotated to connect the port 1 of the PNA to the port 2 of the fixture and vice-versa. Averaging all the S-parameters of the two mea-

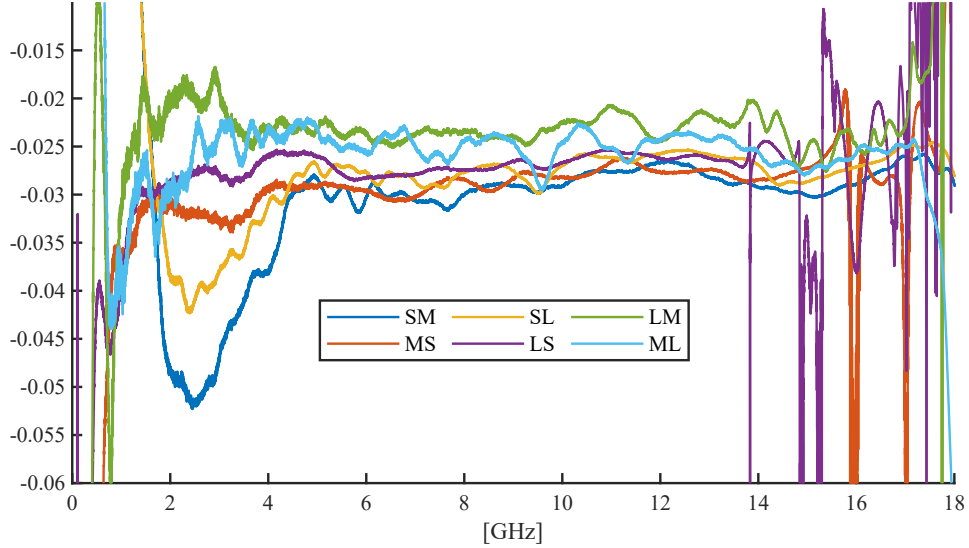


Figure 8: Measured data retrieved effective loss tangent for all the reference-fixture – under-test-fixture combinations.

surements imposes a virtual symmetry condition that effectively removes all differences in the right and left connector adapters for all fixtures alike. An additional averaging is performed before the de-embedding to remove the asymmetries inside each individual test fixture otherwise presenting different S11 and S22. The transmissivity and reflectivity of every fixture for the purpose of de-embedding are then defined as

$$S11 = \frac{1}{4}(S11_a + S11_b + S22_a + S22_b), \quad (4)$$

and

$$S21 = \frac{1}{4}(S21_a + S21_b + S12_a + S12_b), \quad (5)$$

where the subscripts *a* and *b* denote the two PNA measurements made for every fixture.

The de-embedded transmissivity and reflectivity are displayed in Fig. 6. The residual reflection *s* is higher than for the simulated case, but still acceptable especially in X-band (8–12 GHz). Inverting the reference and de-embedded fixture seems to only have a minor effect on the responses.

The effective permittivity in Fig. 7 (derived from the phase component of *t*) is the one showing the largest deviation between pairs of test fixtures. This is probably due to a difference in the permittivity of the two fixtures used in the de-embedding, the error is also amplified in the case of a shorter difference length, as motivated in the next section. Using the results of Section 5 the “LS–SL” and “MS–SM” results are the ones which should better approximate the effective permittivities of the longest of the two lines used

in the de-embedding procedure, i.e. “L” and “M” respectively.

The loss tangent in Fig. 8 also shows some differences, with the measurements “LM–ML” more distant than the other two pairs. Recall, in fact, that the tangent delta is computed from the square root of the dielectric constant (2) and therefore the error will be propagated from one to another.

5 Non-identical fixtures de-embedding error

In the ideal case, the two test fixtures are supposed to have identical propagation constants. In practice, as depicted in Fig. 9, the two lines might have slightly different properties, yielding to an error in the estimation of the electrical length of the virtual line Δ_L in the drawing.

Assuming that the only difference is in the phase velocity of the two lines (and any impedance mismatch between the two lines is negligible), the de-embedding procedures will still be removing the effect of transitions, but also a length of transmission line proportional to $\sqrt{\varepsilon_a} L_a$ (the shortest of the two). The resulting electrical length Δ_L , however, will not be the physical length difference of the two lines but something proportional to the phase delays difference $\propto (\sqrt{\varepsilon_b} L_b - \sqrt{\varepsilon_a} L_a)$. This setup leads to the following estimation for the dielectric constant (1) (e.g., Fig. 7)

$$\sqrt{\varepsilon} = \frac{L_b \sqrt{\varepsilon_b} - L_a \sqrt{\varepsilon_a}}{L_b - L_a} \quad (6)$$

which would not depend on L_b and L_a if $\varepsilon_a = \varepsilon_b$.

Assuming we are interested in finding ε_b , and there is a permittivity error

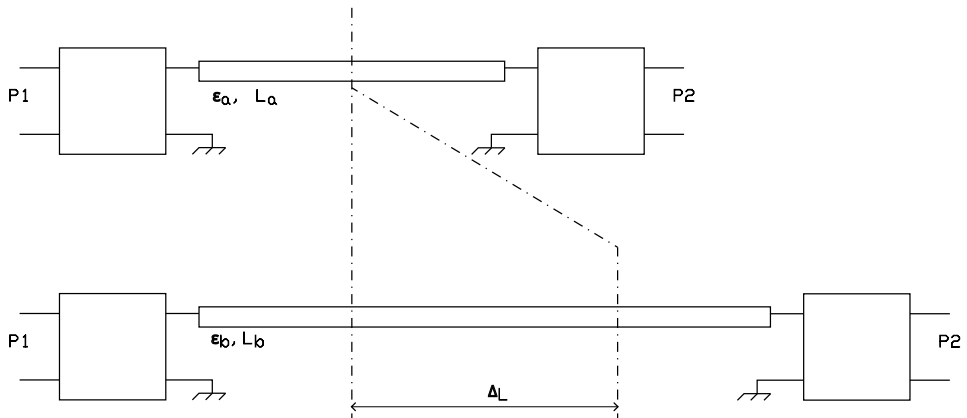


Figure 9: Two-fixtures schematic for the de-embedding procedure. The transitions are identical and the lines are of different lengths to produce a Δ_L -long virtual line response. The error arises from the difference in phase velocity between the two lines (related to the effective permittivities ε).

$\Delta\epsilon$ between the two fixtures such as $\epsilon_a = \epsilon_b + \Delta\epsilon$, the de-embedding result ϵ will deviate from the desired ϵ_b of a quantity

$$\epsilon_{err} = \epsilon_b - \left(\frac{L_b\sqrt{\epsilon_b} - L_a\sqrt{\epsilon_b + \Delta\epsilon}}{L_b - L_a} \right)^2. \quad (7)$$

The error in (7), will be null in the case $\Delta\epsilon = 0$, in the general case we can study its sensitivity to $\Delta\epsilon$ variations

$$\frac{\partial\epsilon_{err}}{\partial\Delta\epsilon} = -\frac{L_a^2}{(L_b - L_a)^2} + \frac{L_b L_a}{(L_b - L_a)^2} \frac{\epsilon_b}{\sqrt{\epsilon_b(\epsilon_b + \Delta\epsilon)}}, \quad (8)$$

which can be further simplified in the case of $\Delta\epsilon \rightarrow 0$ (small perturbations)

$$\frac{\partial\epsilon_{err}}{\partial\Delta\epsilon} \Big|_{\Delta\epsilon=0} = -\frac{L_a^2}{(L_b - L_a)^2} + \frac{L_b L_a}{(L_b - L_a)^2}, \quad (9)$$

exclusively dependent on the line lengths.

The result in (9) tells us that a small error in the phase velocity of two fixtures, will be amplified by the de-embedding algorithm, if $L_b - L_a$ is too small. Furthermore, since (7)(8)(9) all assume $L_b > L_a$, the error from (9) will always be positive for small $\Delta\epsilon$, meaning that ϵ (6) will always be smaller than the measurand ϵ_b .

5.1 Measurement results

Tabulating (9) for the 3 test fixture combinations we obtain Table 2. These values explain the difference in the results in Fig. 7 (and consequently Fig. 8). Also we can say that the measurements “LS–SL” are the ones that best approximate the characteristics of the longest line “L” (due to the smaller error sensitivity), while the measurements “LM–ML” are the worst in this case. By extension, assuming that “LS–SL” and “MS–SM” are good approximations for the properties of “L” and “M” respectively, we still find a difference of ≈ 0.2 in the effective dielectric permittivity indicating a substantial difference between test fixtures.

The dielectric thickness differences measured during the assembly process might be part of the reason for this error. However, varying the thickness of

| L_b [mm] | L_a [mm] | Δ_L [mm] | $\frac{\partial\epsilon_{err}}{\partial\Delta\epsilon}$ |
|------------|------------|-----------------|---|
| 219 | 40 | 179 | 0.22 |
| 219 | 146 | 73 | 2.0 |
| 146 | 40 | 106 | 0.37 |

Table 2: Measurement sensitivity to permittivity variations.

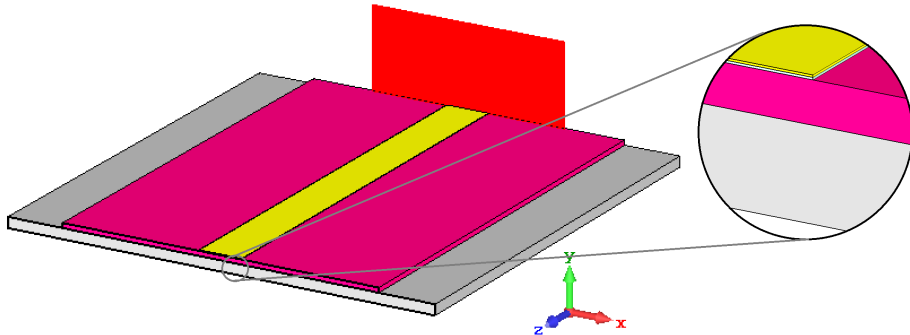


Figure 10: CST model for the microstrip, the layers from top to bottom are: copper 0.03 mm, acrylic 0.03 mm (adhesive), MUT 0.55 mm, aluminium 1.2 mm.

the material in a CST model, doesn't produce a change in ϵ_{eff} large enough to justify the error. Therefore, the reason must lie in some non-homogeneity of the material due to manufacturing errors. In this sense, the measurement "LS–SL" should represent a better *average* of non-idealities effects; and will be used to match a numerical model to the measurement.

6 Numerical model matching

The *LS* measure was fitted to the model in Fig. 10 using the difference of γ (3) ($|\gamma_{sim} - \gamma_{meas}|$) as a frequency-dependent error function. This error curve is integrated over a specified portion of the bandwidth to produce an error value that can be used with an optimizer.

The optimization is performed using a python script that controls the execution of CST and updates the values of the dielectric constant and loss tangent of the MUT between iterations.

The "minimize" function of the library "scipy" is used for the optimization. Different methods can be utilized, the quasi-Newton *BCGF* and the *Nelder-Mead* methods were both found effective (the latter is best if the initial solution is far from convergence). The optimization was performed for X-band (8–12 GHz) and resulted in a material with dielectric permittivity $\epsilon = 3.673$ and a loss tangent $\tan \delta = 0.02754 @ 10$ GHz.

The residual error and the effective permittivity (extended to a 2–17 GHz bandwidth) are plotted in Fig. 11 and Fig. 12 respectively.

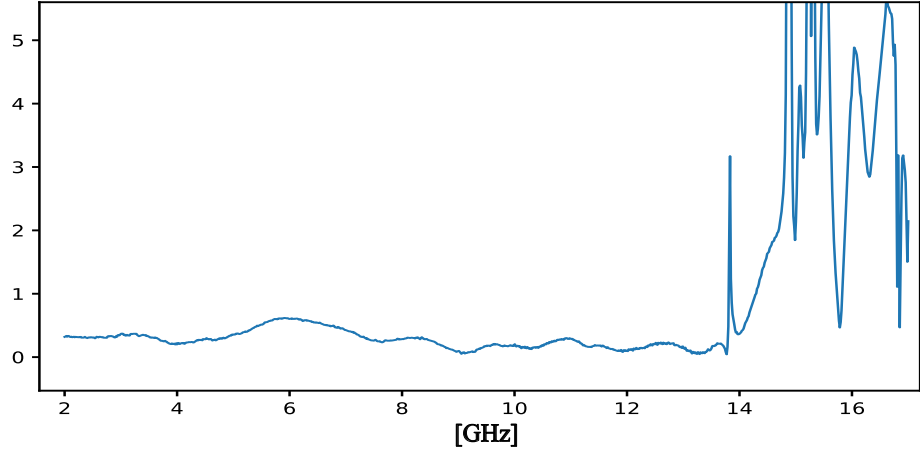


Figure 11: Residual error $|\gamma_{sim} - \gamma_{meas}|$ after optimization, resampled and extended to a 2–17 GHz bandwidth.

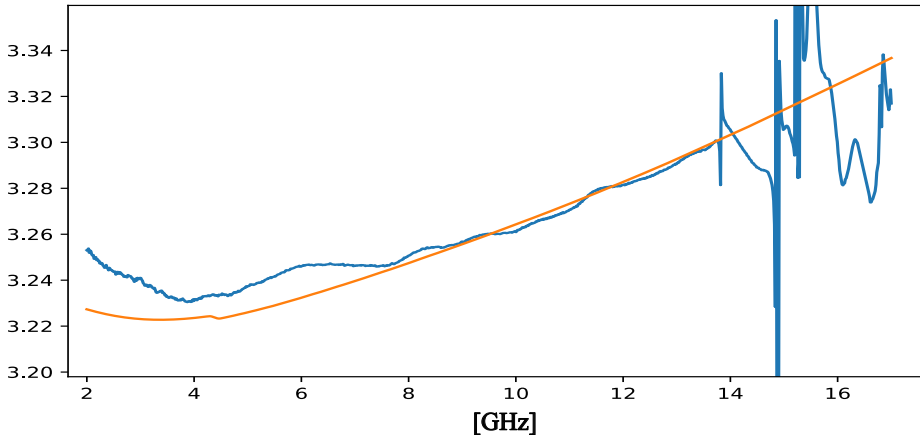


Figure 12: Optimized model (orange) and measurement (blue) ε_{eff} comparison, resampled and extended to a 2–17 GHz bandwidth.

7 Conclusions

The manufacturing process needs to be improved for repeatability. The material is lossy, might still be usable for a reflectarray, definitely not a good choice for traveling-wave antennas. The dielectric constant and thickness shall be used in future simulations to determine the usability in reflectarray cells design.

References

- [1] D. M. Pozar, *Microwave engineering; 3rd ed.* Hoboken, NJ: Wiley, 2005. [Online]. Available: <https://cds.cern.ch/record/882338>